Fully Automated Pipeline for Measurement of the Thoracic Aorta Using Joint Segmentation and Localization Neural Network

Sudeep Katakol[a,b], Zhangxing Bian[c], Yanglong Lu[b], Greg Spahlinger[b], Charles R. Hatt[d], Nicholas S. Burris[b]

[a]Department of Electrical & Computer Engineering, University of Michigan, Ann Arbor, MI, USA
[b]Department of Radiology, University of Michigan, Ann Arbor, MI, USA
[c]Department of Electrical & Computer Engineering, Johns Hopkins University, Baltimore, MD 21218, USA
[d]Imbio Inc, Minneapolis, MN, USA

Abstract.
Purpose: Diagnosis and surveillance of thoracic aortic aneurysm (TAA) involves measuring the aortic diameter at various locations along the length of the aorta, often using computed tomography angiography (CTA). Currently, measurements are performed by human raters using specialized software for 3D analysis, a time-consuming process, requiring 15-45 minutes of focused effort. Thus we aimed to develop a convolutional neural network (CNN)-based algorithm for fully automated and accurate aortic measurements.
Approach: Using 212 CTA scans, we trained a CNN to perform segmentation and localization of key landmarks jointly. Segmentation mask and landmarks are subsequently used to obtain the centerline and cross-sectional diameters of the aorta. Subsequently, a cubic spline is fit to the aortic boundary at the sinuses of Valsalva to avoid errors related inclusions of coronary artery origins. Performance was evaluated on test set of 57 scans, with automated measurements compared against expert manual raters.
Result: Joint training of segmentation and landmark localization tasks yielded higher accuracy for both tasks compared to networks trained for each task individually. Mean absolute error between human and automated was $\leq$ 1 mm at 6 of 9 standard clinical measurement locations. However, higher errors were noted in the aortic root and arch regions, ranging between 1.7 and 2.1 mm, although agreement of manual raters was also lower in these regions.
Conclusion: Fully-automated aortic diameter measurements in TAA are feasible using a CNN-based algorithm. Automated measurements demonstrated low errors that are comparable in magnitude to those with manual raters, however, measurement error were highest in the aortic root and arch.

Keywords: aorta, aneurysm, aortic diameter, segmentation, localization.

*Nicholas S. Burris, nburris@med.umich.edu

1 Introduction

Thoracic aortic aneurysm (TAA) is a common disease affecting between 1 – 3% of the US population over the age of 50, which is characterized by enlargement of the largest artery in the body (i.e., the thoracic aorta) as a result of weakening of the aortic wall.[1] TAA is a largely silent disease until potentially fatal complications such as rupture occur. Patients with TAA undergo regular surveillance imaging using computed tomography angiography (CTA) to monitor the overall size of their aneurysm and to detect growth, assessments which in turn determine the need for surgical

repair.[2] Aortic diameter measurements are used to assess TAA, with measurements performed on volumetric CTA imaging data by manual analysts (i.e., technologists or the physicians themselves) using dedicated 3D image rendering software. Diameter measurements are made in standardized anatomic locations along the length of the aorta to minimize measurement variability and ensure comparability of measurements across time.[3,4]

Currently, such measurements are performed manually by human raters, either technologists or physicians, using 3D image analysis software. This process in time and labor intensive, requiring between 15 and 45 minutes of focused effort to generate a complete set of measurements depending on the complexity of pathology. TAAs typically grow at very slow rates, and aortic diameters typically only enlarge by 1-3 millimeters between surveillance imaging exams,[5] meaning that significant effort is required on the part of the human rater to ensure accurate diagnostic information. The rigorous and repetitive nature of this task can lead to fatigue in human raters, comprising measurement accuracy and speed.

To overcome this limitation, we sought to develop a Machine Learning (ML) based algorithm that allows us to obtain aortic measurements in a fully automated fashion. Our current method builds on recent work involving the use of Convolutional Neural Networks (CNNs) to segment[6] and localize key anatomic landmarks on the aorta.[7] Specifically, in this work we aimed to develop a CNN *simultaneously* that performs joint aortic segmentation and landmark localization, and subsequently use the output of this network to generate an aortic centerline and extract maximal cross-section diameters at points along the centerline corresponding to the standard clinical measurement locations.

2 Method

2.1 Pipeline

The objective of our automated measurement pipeline is to extract aortic diameter measurements at 9 standard aortic locations used clinically,[3,4] however, we achieve this through localization of 6 landmarks, from which 3 additional measurement locations are derived. These six landmarks are: center of the aortic valve (L1); proximal arch (L2); just distal to the left subclavian artery (L3); celiac artery (L4); mid-arch (L5); and sinotubular junction (L6). Three additional measurements at standard locations are derived from these 6 landmarks including: Mid Ascending aorta (mid between the sinotubular junction and proximal arch), 2cm distal to the left subclavian artery (along the centerline), and 2 cm proximal to celiac artery (along centerline). To obtain the aortic measurements from a given CT scan I, we begin by reorienting the CT image and rescaling it to have isotropic unit-spacing. We input this standardized CT image to a convolutional neural network (CNN) which segments the aorta and localizes ($L = 6$) landmarks of interest. Using the landmarks and segmentation, we estimate an aortic centerline as well as cross-sections along it. The diameters of the cross-section closest to desired locations are output.

2.2 Dataset and training details

We collected 212 CTA scans, of which 155 scans from 57 unique patients were used for training the joint segmentation-localization CNN, and 57 scans from 15 patients were used for testing. Aortic measurements were performed in the test scans at standard anatomic locations by three independent expert analysts, with the average value between raters used to define the ground truth measurements against which the output of the fully-automated approach was compared. This retrospective study was performed as part of an Institutional Review Board (IRB), HIPAA-compliant

study (HUM00133798) with a waiver of informed consent at the University of Michigan, Ann Arbor, Michigan.

2.3 CNN-based joint segmentation and localization

Our CNN is tasked to perform both segmentation and localization. The network utilizes a UNet[8] stem (with shared parameters θ) f_θ^{shared} and two separate branches g_ϕ^{seg} and g_ψ^{ll} for segmentation and landmark localization respectively (Figure 1).

The probability of each voxel being a point inside the aorta is estimated as $g_\phi^{\text{seg}}(f_\theta^{\text{shared}}(I)) \in [0,1]^{H\times W\times D}$. Similarly, $g_\psi^{\text{ll}}(f_\theta^{\text{shared}}(I)) \in [0,1]^{L\times H\times W\times D}$ is a vector such that $g_\psi^{\text{ll}}(f_\theta^{\text{shared}}(I))(l,h,w,d)$ contains the probability that the voxel at (h,w,d) contains the landmark indexed by l.

Landmark localization is learned via heatmap regression.[9] However, instead of using the MSE loss typically used for heatmap regression, we use a weighted cross-entropy (WCE) loss that was found to stabilize training and improve accuracy.[7] Given ground truth landmarks $L_l^* \in \mathbb{R}^3$ for each landmark l in a given image I, the landmark localization loss is calculated as

$$\begin{aligned}\mathcal{L}^{ll} &= \text{WCE}(\hat{y}_{\text{ll}}, y^{\text{ll}}; \alpha) \\ &= \frac{-1}{LHWD}\sum_{l,h,w,d}\left[\alpha\, y^{\text{ll}}(l,h,w,d)\log\left(\hat{y}_{\text{ll}}(l,h,w,d)\right) + (1-\alpha)\left(1-y^{\text{ll}}(l,h,w,d)\right)\log\left(1-\hat{y}_{\text{ll}}(l,h,w,d)\right)\right]\end{aligned}$$

where $y^{ll}(l,h,w,d) = \exp\left(\frac{\left\|[h,w,d]^T - L_l^*\right\|_2^2}{2\sigma^2}\right)$ and $\hat{y}_{\text{ll}} = g_\psi^{\text{ll}}(f_\theta^{\text{shared}}(I))$. In order to prevent the network from collapsing into the trivial all-zero local minimum solution and to promote predictions of positive values, we employ a high alpha value (> 0.5) in the loss function.

Binary cross-entropy was used for segmentation loss $\mathcal{L}^{seg}$. Thus, the total loss optimized by the network is $\mathcal{L}^{seg} + \lambda L^{ll}$ where λ balances the contribution of each of the two losses.

We trained our network with randomly cropped CT images augmented by performing small random rotations, using a $\sigma = 12.5$ for 100 epochs and then a decaying σ with a rate of 0.98 (i.e., $\sigma_{t+1} = 0.98\sigma_t$) for another 100 epochs. λ was set to 10 and α was set to 0.9.

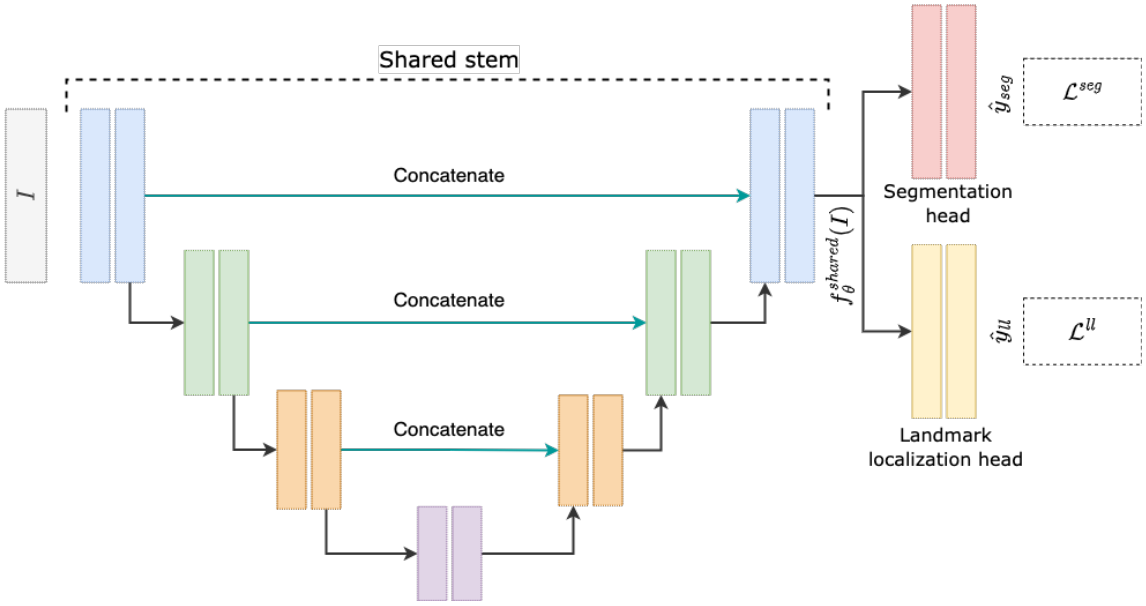

Fig 1: The architecture of the CNN used. We have a UNet stem that branches out into separate heads for each task, i.e., segmentation and landmark localization.

2.4 Post-processing

Following inference, the final aorta segmentation was taken as the largest connected component from the CNN's segmentation output.

2.5 Aortic measurements

2.5.1 Centerline generation

To determine the centerline of the aorta, the aorta was first skeletonized.[10] The skeleton often has branches in the aortic root and branch vessels. To reduce this to a single branch, we first found

points on the skeleton nearest to the sinotubular junction and celiac landmarks. Next the original skeleton was converted to it's connected graph representation. Finally, shortest path between the sinotubular junction and celiac points was found using Dijkstra's algorithm.[11] The resulting endpoints and the shortest path between them become the final centerline.

2.5.2 Aortic cross-section localization

The center of each cross-section at the the sinotubular junction, proximal arch, mid-arch and celiac was determined by finding the centerline point nearest to the corresponding landmark point inferred from the CNN. For the measurement at 2 cm distal to left subclavian, we find the closest centerline point to the left subclavian landmark and move 2 cm distal along the centerline. We perform a similar measurement 2 cm proximal to celiac artery landmark. The half-way point along the centerline between the STJ (L6) and proximal arch (L2) defines the location for mid ascending measurements. Similarly, the mid-descending measurement is obtained by moving along the centerline to halfway between the left subclavian (L3) and celiac (L4) arteries.

The vector normal to each cross-section was estimated as the difference between the coordinates of the two neighboring centerline points.

2.5.3 Sinuses of Valsalva measurement

The Sinuses of Valsalva (SVS) are the widest part of the aortic root, and represent the first aortic segment beyond the aortic valve (L1). To obtain the SVS measurement, we considered all the centerline points between the aortic annulus and the STJ. The maximal diameters at each of these points were considered and the highest was reported as the SVS measurement. In some cases, the cross-sections can include one or both of the coronary arteries, leading to overestimation of

diameter measurements. To alleviate this issue, we employed a technique to remove the proximal coronary arteries from the SVS cross-section. First, fit a cubic spline to the boundary of the plane and estimated the curvature at various points on the boundary, which are indicative of branch vessels. We then removed the 5 points with the highest curvature from original boundary and found a new boundary by fitting a linear spline on the remaining points.

3 Results

3.1 Benefits of Multi-task training

Multi-task learning has been shown to improve generalization of deep-neural networks.[12] To demonstrate this for our application, we performed a experiment comparing our network trained for joint segmentation and localization against ones trained exclusively for segmentation and localization. Note that only L1-L4 landmarks were considered in this experiment. As expected, the multi-tasked model performed better on both segmentation and localization tasks as shown in Table 1.

	Segmentation (DICE)	Localization (euclidean dist. in mm)				
		L1	L2	L3	L4	Avg.
Individual	94.70	14.2	8.2	5.6	20.5	12.1
Ours (Multi-task)	**97.16**	**4.4**	**3.9**	**2.4**	**4.4**	**4.3**

Table 1: Performance comparison of the Multi-task model against separate models trained exclusively for segmentation and landmark localization. Refer to Figure 3 for visualization of L1-L4.

3.2 Comparison of automated measurements against human raters

We compared the aortic measurements obtained via our method against the average measurements from three raters. It was observed that the mean absolute difference between measurements were $\leq$ 1 mm at 6 of 9 aortic locations, but ranged from 1.7-2.1 mm at the SVS, STJ and Mid Arch

locations, as shown in Table 2. Mean absolute error was highest at the SVS (1.69 mm), STJ (2.07 mm) and Mid arch (1.85 mm), although the standard deviation of manual rater measurements was also highest in these locations (1.2 mm, 1.8 mm and 1.2 mm respectively). Bias was $<$1 mm at all locations, with our automated approach demonstrating a small degree of systematic over-measurement in the SVS and STJ, whereas in all other aortic locations the automated approach slightly overestimated aortic measurements relative to manual raters. Representative examples of segmentation, landmark localization and measurement planes are visualized in Figure 3. Bland-Altman plots showing the difference between the gold-standard manual diameter measurements (average of 3 raters) and automated diameter measurements for all landmarks are shown in Figure 2.

We note that the average time taken by the rater is 24 minutes (range: 15-38 minutes), while our method takes about 15 seconds per CTA scan on a standard high-performance laptop with a GPU.

Location	Mean Abs. Error (in mm)	Bias (in mm)	95 %ile range (in mm)	Rater Std. dev. (in mm.)
Sinuses of Valsalva (SVS)	1.7	-0.7	[-4.8, 3.5]	1.2
Sinotubular junction (STJ)	2.1	-0.3	[-5.6, 5.0]	1.8
Mid Ascending	0.6	0.0	[-1.4, 1.4]	0.7
Proximal Arch	1.0	0.7	[-1.5, 3.0]	1.2
Mid Arch	1.9	0.7	[-4.7, 6.2]	1.2
2cm distal to Left Subclavian	0.9	0.6	[-1.6, 2.9]	1.0
Mid Descending	0.8	0.1	[-2.9, 3.1]	1.0
2cm proximal to Celiac	0.7	0.5	[-1.4, 2.4]	0.9
Celiac Artery	0.8	0.2	[-1.8, 2.2]	0.7

Table 2: Comparison of the diameter measurements from ML method versus average measurements from three expert raters by aortic location. The first column reports the mean absolute error between automated and manual diameters. The second column reports the average difference (bias) between rater-measured and algorithm-output diameters (actual minus predicted). The third column reports the 95th percentile range of the measurement error. The fourth column report the average standard deviation in manual diameter measurement for comparison.

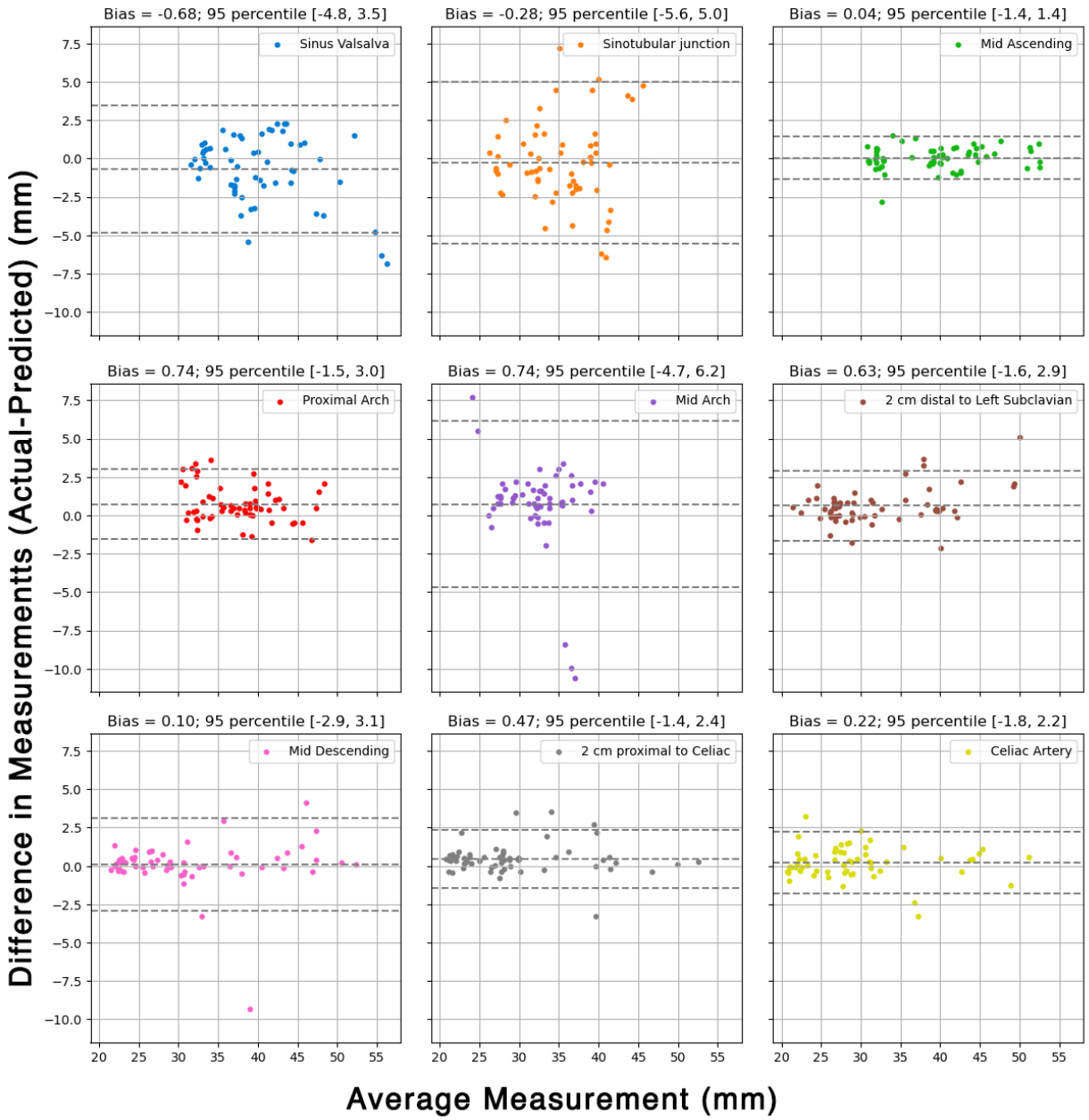

Fig 2: Bland-Altman plots showing the difference between actual (average of 3 expert raters) and predicted diameter measurements for at all nine standard aortic measurement locations.

3.3 Effect of Sinus Valsalva correction

We observe that the mean absolute error reduces from 1.96 mm to 1.69 mm after including the sinus valsalva correction process. A visualization of the procedure of correction and its effects is shown in Figure 4.

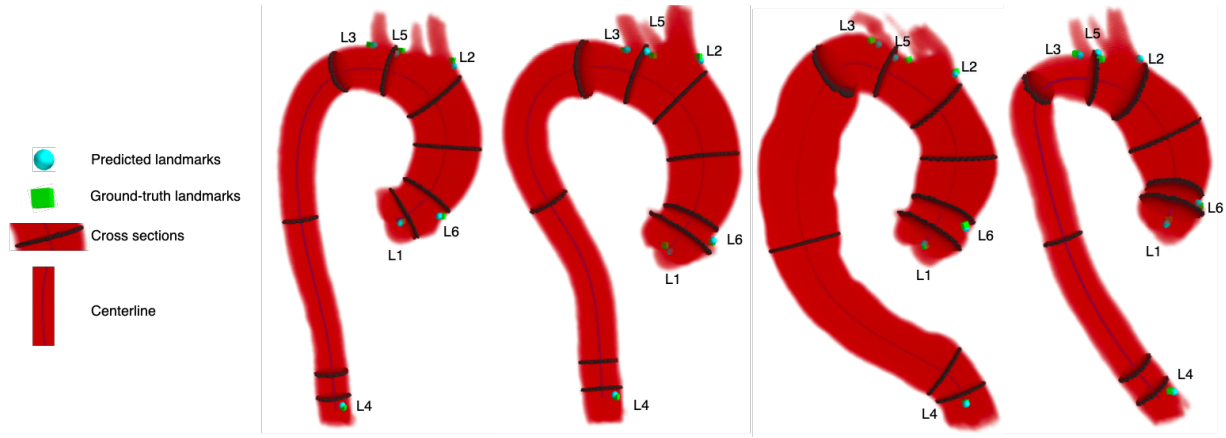

	Predicted	Actual	Predicted	Actual	Predicted	Actual	Predicted	Actual
Sinus Valsalva	36.6	36.5	38.0	36.1	38.0	36.2	32.8	33.2
Sinotubular junction	33.1	30.7	32.5	31.7	37.2	35.5	30.0	31.0
Mid Ascending	39.1	38.8	39.0	38.7	41.6	42.4	40.2	40.3
Proximal Arch	37.4	37.4	39.3	39.3	35.0	35.7	32.5	32.2
Mid Arch	28.6	29.8	33.4	32.9	28.6	29.5	26.9	26.1
2 cm distal to Left Subclavian	24.9	24.7	31.7	31.7	34.2	36.9	21.1	21.7
Mid Descending	22.1	22.3	24.1	24.5	42.2	42.7	21.6	21.4
2 cm proximal to Celiac	21.4	21.9	23.9	24.0	32.5	34.4	22.9	23.1
Celiac Artery	21.9	22.4	23.9	24.6	30.2	31.0	22.6	22.5

Fig 3: Representative cases demonstrating predicted segmentation, ground-truth and predicted landmarks, aortic centerline, cross-sectional measurement planes, and extracted diameter Predicted and Actual diameter measurements. We demonstrate that our automated approach yields accurate landmark localization and aortic diameter measurements across a range of aortic geometries including: mild ascending dilation (left), mild ascending dilation with tortuosity and bovine arch (center left), arch and descending dilation with tortuosity (center right), and mild ascending dilation with acute arch angulation and bovine arch (right).

4 Conclusion

We demonstrate a simple and rapid ML-based method to obtain automated aortic measurements using a CNN trained for segmentation and landmark localization, and show that added accuracy is attained by joint training a single CNN to perform both tasks simultaneously. The obtained diameter measurements errors were within 1 mm of human reported diameters at the majority of the nine locations analyzed, although errors were higher (1.5-2 mm) at the SVS, STJ and mid arch, locations which are characterized by more irregular aortic contours and rapid changes in diameter over short lengths(Figure 5. It is important to note that the variance of expert manual rater measurements was also the highest at these locations, supporting prior reports suggesting that these anatomic locations are the more challenging to reproducibly measure due to their anatomy.[13] When compared to a

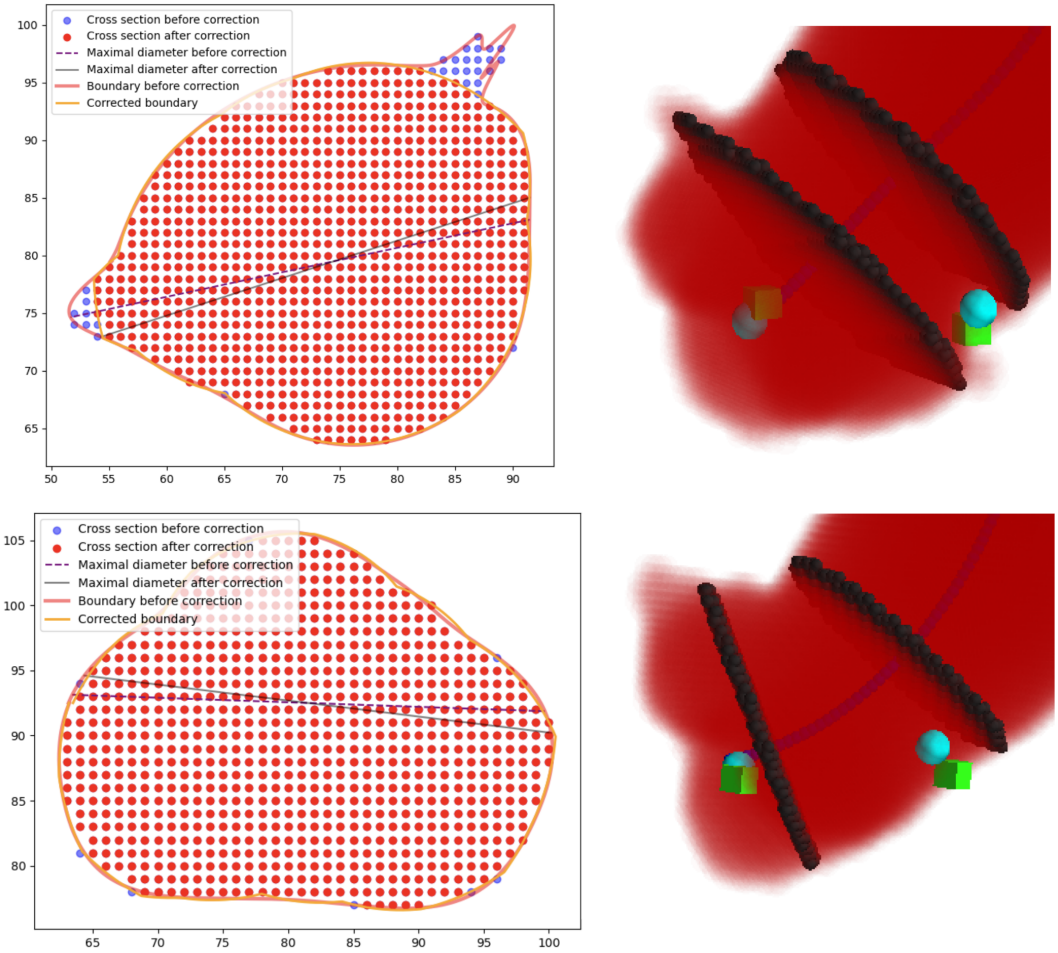

Fig 4: Visualization of the results of our cubic spline process refining the aortic boundary at the sinuses of Valsalva (as described in Section 2.3.3). We demonstrate that correction happens only when branching coronary arteries are present in the selected aortic cross-section (top left) and not when absent (bottom left). Corresponding segmentation results of the aortic root with predicted (teal sphere) and ground-truth (green cube) L1 and L6 landmarks are also shown (right).

similar, recently described deep learning pipeline for automated aortic measurement, our pipeline performed substantially better (e.g., 95th percentile errors of about 5 mm in our study compared to 10 mm in prior reports[14,15]). However, these prior reports evaluated a more heterogeneous patient population including pathologies other than aortic aneurysm (e.g., aortic dissection), which can dramatically alter aortic geometry and contrast levels.

The results of our work have potential practical applications for daily clinical analysis. First, the fully automated process we describe in this work could obviate the need for significant human

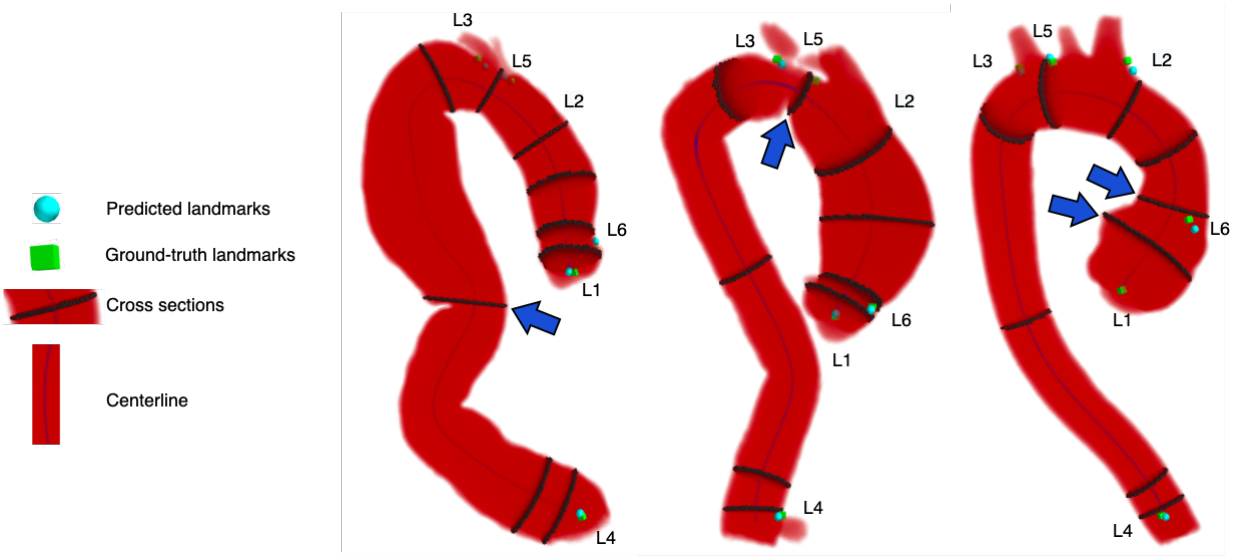

	Predicted	Actual	Predicted	Actual	Predicted	Actual
Sinus Valsalva	31.7	31.3	33.6	34.3	50.1	46.4
Sinotubular junction	28.7	26.5	34.2	33.5	37.0	41.4
Mid Ascending	36.4	36.5	51.2	50.6	31.9	31.8
Proximal Arch	32.3	35.9	39.0	39.0	30.1	33.2
Mid Arch	27.4	29.1	22.0	27.5	32.4	32.3
2 cm distal to Left Subclavian	41.1	39.0	29.0	28.7	28.9	29.0
Mid Descending	43.6	34.3	28.9	29.1	27.1	27.5
2 cm proximal to Celiac	41.3	38.0	27.9	28.3	25.4	25.9
Celiac Artery	39.8	40.3	27.4	28.3	26.0	25.6

Fig 5: Representative cases where there was substantial disagreement between predicted measurements and actual measurements from expert raters at a specific aortic location (blue arrow). Disagreements tended to occur in aortic segments with irregular anatomy characterized by tortuously and/or rapidly changing diameter along the ceterline. Shown is a case with a 9.3 mm discrepancy at the mid-descending level (left), a case with a 5.5 mm discrepancy at the mid-arch (middle), and a case with up to 4.4 mm discrepancy at the SVS and STJ (right).

effort spent performing the tedious and repetitive task of standardized aortic measurement. In clinical practice we expect that some human interaction will still be required to verify the results of automated analysis and correct any erroneous measurements. However, the substantial time savings of an automated approach (i.e., 15 seconds compared to at least 15 minutes) promises to allow substantial human effort to be re-distributed to higher-level diagnostic tasks, a potentially impactful change given increasing productivity demands and rates of burnout in diagnostic radiology.[16,17] Such Furthermore, many smaller hospitals do not have resources to support aortic measurement work in a dedicated 3D laboratory, and thus an automated solution such as the one we describe may facilitate broader availability of high-quality and comprehensive aortic measurements for patients

with TAA.

In conclusion, we present a fully automated pipeline for accurate and comprehensive thoracic aortic measurement in patients with TAA using CTA data and a joint localization and segmentation CNN. Our automated pipeline results in significant time saving for aortic diameter analysis, with measurement results that are comparable to that of expert manual raters in most instances. However, measurement accuracy remains suboptimal at regions highly variable aortic anatomy such as the SVS and mid-arch, although these regions are also challenging for human raters. Future effort will focus on further refining our automated processes to address current inaccuracies as well as expanding the applicability our pipeline to non-gated, and potentially non-contrast CTA imaging, as well as more diverse types of aortic pathology.

Disclosures

Charles Hatt is an employees of and has stock options in Imbio Inc. Nicholas Burris is entitled to royalties related to licensure of intellectual property to Imbio Inc. No other authors have any relevant disclosures.

Acknowledgments

We would like to acknowledge Melissa Muck, Robyn Wright and Eric Wizauer for their contribution to this research. This work is based on a conference paper titled ”Fully automated aortic measurements via CNN-based joint segmentation and localization”, presented at SPIE Medical Imaging 2023.

References

1 M. Mori, S. U. B. Mahmood, S. Yousef, *et al.*, "Prevalence of incidentally identified thoracic aortic dilations: insights for screening criteria," *Canadian Journal of Cardiology* **35**(7), 892–898 (2019).

2 K. G. Kallianos and N. S. Burris, "Imaging thoracic aortic aneurysm," *Radiologic Clinics* **58**(4), 721–731 (2020).

3 L. Hiratzka, G. Bakris, J. Beckman, *et al.*, "2010 accf/aha/aats/acr/asa/sca/scai/sir/sts/svm guidelines for the diagnosis and management of patients with thoracic aortic disease," *Journal of the American College of Cardiology* **55**(14), e27–e129 (2010).

4 A. F. Members, S. D. Kristensen, J. Knuuti, *et al.*, "2014 esc/esa guidelines on non-cardiac surgery: cardiovascular assessment and management: The joint task force on non-cardiac surgery: cardiovascular assessment and management of the european society of cardiology (esc) and the european society of anaesthesiology (esa)," *European heart journal* **35**(35), 2383–2431 (2014).

5 D. Oladokun, B. Patterson, J. Sobocinski, *et al.*, "Systematic review of the growth rates and influencing factors in thoracic aortic aneurysms," *European Journal of Vascular and Endovascular Surgery* **51**(5), 674–681 (2016).

6 J. Zhong, Z. Bian, C. R. Hatt, *et al.*, "Segmentation of the thoracic aorta using an attention-gated U-Net," in *Medical Imaging 2021: Computer-Aided Diagnosis*, M. A. Mazurowski and K. Drukker, Eds., **11597**, 115970M, International Society for Optics and Photonics, SPIE (2021).

7 Z. Bian, J. Zhong, Y. Lu, *et al.*, "LitCall: learning implicit topology for CNN-based aortic

landmark localization," in *Medical Imaging 2022: Image Processing*, O. Colliot and I. Išgum, Eds., **12032**, 120320X, International Society for Optics and Photonics, SPIE (2022).

8 O. Ronneberger, P. Fischer, and T. Brox, "U-net: Convolutional networks for biomedical image segmentation," in *International Conference on Medical image computing and computer-assisted intervention*, 234–241, Springer (2015).

9 C. Payer, D. Štern, H. Bischof, *et al.*, "Integrating spatial configuration into heatmap regression based cnns for landmark localization," *Medical Image Analysis* **54**, 207–219 (2019).

10 T. C. Lee, R. L. Kashyap, and C.-N. Chu, "Building skeleton models via 3-d medial surface/axis thinning algorithms," *Computer Vision, Graphics, and Image Processing* **56**(6), 462–478 (1994).

11 E. W. Dijkstra, "A note on two problems in connexion with graphs," in *Edsger Wybe Dijkstra: His Life, Work, and Legacy*, 287–290 (2022).

12 S. Ruder, "An overview of multi-task learning in deep neural networks," *arXiv preprint arXiv:1706.05098* (2017).

13 F. M. Asch, E. Yuriditsky, S. K. Prakash, *et al.*, "The need for standardized methods for measuring the aorta: multimodality core lab experience from the gentac registry," *JACC: Cardiovascular Imaging* **9**(3), 219–226 (2016).

14 M. Pradella, T. Weikert, J. I. Sperl, *et al.*, "Fully automated guideline-compliant diameter measurements of the thoracic aorta on ecg-gated ct angiography using deep learning," *Quantitative Imaging in Medicine and Surgery* **11**(10), 4245 (2021).

15 C. B. Monti, M. van Assen, A. E. Stillman, *et al.*, "Evaluating the performance of a convo-

lutional neural network algorithm for measuring thoracic aortic diameters in a heterogeneous population," *Radiology: Artificial Intelligence* **4**(2), e210196 (2022).

16 C. Liew, "The future of radiology augmented with artificial intelligence: a strategy for success," *European journal of radiology* **102**, 152–156 (2018).

17 B. Spieler and N. Baum, "Burnout: a mindful framework for the radiologist," *Current Problems in Diagnostic Radiology* **51**(2), 155–161 (2022).

Sudeep Katakol is a 2022 graduate from Univ. Of Michigan with a Master's degree in Electrical and Computer Engineering. He received his Bachelor's degrees in Computer Science as well as Mathematics from BITS Pilani, Goa, India. His current interests lie in Computer Vision, especially in the field of Generative AI.

Zhangxing Bian is a PhD student at Johns Hopkins University. He received his BS from Southeast University in China in 2019 and MS degree in University of Michigan in 2021. His research interests include medical image analysis and machine learning.

Yanglong Lu is Assistant Professor at the Hong Kong University of Science and Technology. He received his BS and PhD from Georgia Institue of Techology in 2020. His research interests include multi-physics modeling and machine learning applications in manufacturing.

Gregory Spahlinger is Research Analyst at University of Michigan. He received his BS at Guilford College in 2006 and his PhD in Chemistry at Michigan State University in 2014.

Charles Hatt is Research Director and Senior Scientist at Imbio Inc and Adjunct Research Professor at University of Michigan. He received his BSE and MSE at Univeristy of Michigan in 2005

and his PhD in Biomedical/Medical Engineering at University of Wisconsin-Madison in 2015.

Nicholas Burris is Assistant Professor of Radiology at at University of Michigan. He received his BS at University of Maryland, Baltimore County in 2006 and his MD from University of Maryland in 2010. His research interests include aortic imaging, medical image analysis and translational research.

List of Figures

List of Tables

2 Comparison of the diameter measurements from ML method versus average measurements from three expert raters by aortic location. The first column reports the mean absolute error between automated and manual diameters. The second column reports the average difference (bias) between rater-measured and algorithm-output diameters (actual minus predicted). The third column reports the 95th percentile range of the measurement error. The fourth column report the average standard deviation in manual diameter measurement for comparison.